The σ- and π-Bonding Modes of a Tetraanionic Porphyrinogen Ligand in Zirconium(IV) Complexes: a Theoretical Investigation†

Angela Rosa,*[a] Giampaolo Ricciardi,[a] Marzio Rosi,[b] Antonio Sgamellotti[b] and Carlo Floriani[c]

[a] *Dipartimento di Chimica, Universitá della Basilicata, Via N. Sauro 85, 85100 Potenza, Italy*
[b] *Dipartimento di Chimica, Universitá di Perugia, Via Elce di Sotto 8, 06100 Perugia, Italy*
[c] *Section de Chimie, Université de Lausanne, Place du Château 3, CH-1005 Lausanne, Switzerland*

The bonding modes of the porphyrinogen ligand L^{4-} (H_4L = 5,10,15,20,22,24-hexahydroporphyrin) with the metal ion Zr^{4+} are analysed in detail for the limiting co-ordinations $\eta^5,\sigma,\eta^5,\sigma$ and $\sigma,\sigma,\sigma,\sigma$. It is concluded that in both co-ordination modes σ bonding is by far the most dominant, mainly due to strong charge donation from the pyrrolic nitrogen lone pairs into the empty $4d_{x^2-y^2}$ and $4d_{xz}$, with additional effects from donation into the $4d_{z^2}$ and 5s orbitals. The π bond, resulting from donation from occupied pyrrolyl π orbitals into the metal $4d_{xy}$ and $4d_{yz}$ orbitals is significant for $\eta^5,\sigma,\eta^5,\sigma$- but rather weak for $\sigma,\sigma,\sigma,\sigma$-co-ordination due to the diminished donation into the $4d_{xy}$ orbital. The total orbital interaction contribution (the covalent component) is about one third of the ionic component of the bond, the latter being identified as the sum of the Pauli repulsion and the attractive electrostatic interaction between L^{4-} and Zr^{4+}. The ionic contribution is about the same in the two configurations, but the covalent component of the bond decreases by *ca.* 3 eV for $\sigma:\sigma:\sigma:\sigma$ co-ordination due mostly to a weaker π-bond interaction. The $\eta^5,\sigma,\eta^5,\sigma$ complex is only 2.1 eV more stable, indicating that the interconversion between the two co-ordination modes is a relatively easy process. The most stable co-ordination mode is preserved after interaction of the substrate with the Lewis bases tetrahydrofuran or H^-.

Although porphyrinogen (5,10,15,20,22,24-hexahydroporphyrin (H_4L) is a well known precursor of porphyrin, its chemistry has never been explored. This is mainly due to its instability since it spontaneously forms porphyrin,[1-3] the oxidation reaction being facile due to the presence of hydrogen atoms in the *meso* (5,10,15,20-) positions. However, a stable form of porphyrinogen has been known for more than a century,[4] with alkyl groups at each *meso* position.[4] Recent investigations by Floriani and co-workers on the use of 5,5,10,10,15,15,20,20-octaalkylporphyrinogen in co-ordination and organometallic chemistry led to the discovery of some peculiar characteristics.[5-8] (*i*) The tetraanionic form of the octaalkylporphyrinogen stabilizes high-valent metals, as in iron(III) and oxomolybdenum(V) complexes.[5] (*ii*) The conformational flexibility allows for close proximity between the peripheral aliphatic chains and the metal.[5,6] (*iii*) The tetraanionic form of the octaalkylporphyrinogen undergoes a reversible redox process involving the formation and cleavage of cyclopropane units,[7] equation (1) (R = alkyl). (*iv*) The four

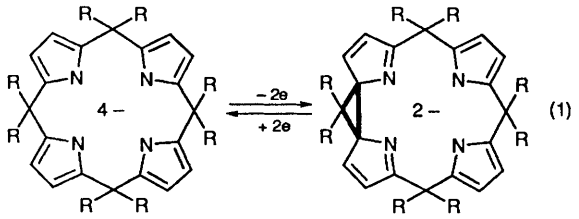

(1)

independent and conformationally flexible pyrrole anions can bind the metal in a σ-, η^3- or η^5-fashion providing $4(n + 2)$ electrons ($0 \leqslant n \leqslant 4$) for the metal (with the following contribution for each pyrrole anion: σ, $n = 0$; η^3, $n = 0.5$; η^5, $n = 1$) depending on the requirement during the reaction pathway.[8]

† *Non-SI units employed:* a_0 5.292 × 10^{-11} m, eV ≈ 1.60 × 10^{-19} J

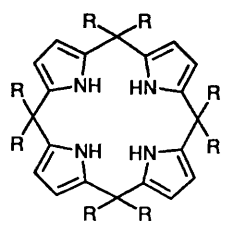

H_4L (R = H)

(*v*) The pyrrolyl anions σ bonded to the central metal atom maintain the ability to bind in a η^3 or η^5 fashion to another metal ion on the periphery of the ligand, as in $[ML'Li_2(thf)]$ **1** (M = Fe, Co or Cu, H_4L' = 5,5,10,10,15,15,20,20-octaethylporphyrinogen, thf = tetrahydrofuran).[6]

The present theoretical study is essentially concerned with the relationship between the σ- and π-bonding modes of the four independent pyrrolyl anions with d^0 transition metals. The model compound chosen is [ZrL], which was isolated as an adduct with different Lewis bases, *i.e.* [ZrL]·X [X = thf, H^- or R^- (R = σ-alkyl)]. There are a number of questions arising from the chemical behaviour of such model compounds.

First, how can we depict the electronic configuration of the metal for the two limiting cases $\sigma,\sigma,\sigma,\sigma$ *vs.* $\eta^5,\sigma,\eta^5,\sigma$ co-ordination and what is the energy barrier between the two? Secondly, how is the bonding mode of the porphyrinogen affecting the Lewis acidity of the metal? Thirdly, how can the addition of a Lewis base to the metal affect the bonding mode of the porphyrinogen?

To answer these questions, we shall make extensive use of an energy decomposition scheme (see later) which, combined with a fragment formalism, has proven itself a useful tool in the analysis of the bonding mechanism in other organometallic compounds.[9] This scheme allows us to separate the steric

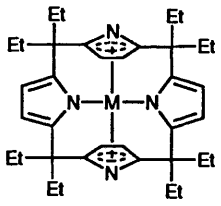

$\eta^5,\sigma,\eta^5,\sigma$

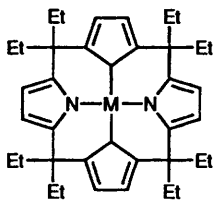

$\sigma,\sigma,\sigma,\sigma$

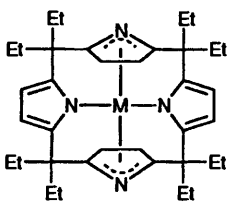

$\eta^3,\sigma,\eta^3,\sigma$

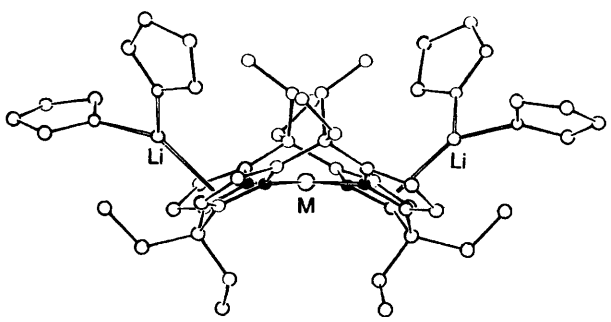

1

factors from the orbital-interaction contributions. The latter are broken down according to the irreducible representations of the point group (C_{2v}), which affords a quantitative estimate of the σ- and π-bond strengths.

Computational Procedure

The calculations reported in this paper are based on the Amsterdam CF program package[10,11] characterized by the use of a density-fitting procedure to obtain accurate Coulomb and exchange potentials in each self-consistent field (SCF) cycle, by accurate and efficient numerical integration of the effective one-electron Hamiltonian matrix elements and by the possibility of freezing core orbitals. The LSD exchange potential was used,[12] together with the Vosko–Wilk–Nusair[13] parametrization for correlation, including Stoll's correction for correlation between electrons of different spin.[14] The molecular orbitals were expanded in an uncontracted double-ζ Slater-type orbital (STO) basis set for all atoms with the exception of the 4d Zr orbital for which we used a triple-ζ STO basis set. As polarization functions one 5p STO was used for Zr. The cores (Zr: 1s,2p; N,C,O: 1s) were kept frozen. Bond energies included Becke's non-local correction[15] to the local exchange expression. Excellent metal–metal and metal–ligand bond energies are obtained from this density-functional based approach as shown by calculations on metal carbonyls,[16] binuclear metal complexes,[17] alkyl and hydride complexes,[18] as well as complexes containing a metal–ligand bond for a number of different ligands.[19]

In order to analyse the interaction energies between the considered fragments, we use a method that is an extension of the well known decomposition scheme of Morokuma.[20] The bonding energy is decomposed into a number of terms. The first term, ΔE^0, is obtained from the energy of the wavefunction ψ^0 which is constructed as the antisymmetrized and renormalized product of the wavefunctions ψ^A and ψ^B of the fragments A and B, as outlined in equations (1)–(5). The term ΔE^0, which is

$$\psi^0 = NA\{\psi^A\psi^B\} \quad (1)$$

$$E^0 = \langle\psi^0|H|\psi^0\rangle \quad (2)$$

$$E^A = \langle\psi^A|H^A|\psi^A\rangle \quad (3)$$

$$E^B = \langle\psi^B|H^B|\psi^B\rangle \quad (4)$$

$$\Delta E^0 = E^0 - E^A - E^B = \Delta E_{\text{elstat}} + \Delta E_{\text{Pauli}} \quad (5)$$

appropriately called the steric repulsion,[21] consists of two components. The first is the electrostatic interaction ΔE_{elstat} of the nuclear charges and unmodified electronic-charge density of one fragment with those of the other fragment, both fragments being at their final positions. Usually ΔE_{elstat} is negative, *i.e.* stabilizing. The second component is the so-called exchange repulsion or Pauli repulsion ΔE_{Pauli}.[22,23] This is essentially due to the antisymmetric requirement on the total wavefunction, or equivalently the Pauli principle, which leads to a depletion of electron density in the region of overlap between ψ^A and ψ^B and an increase in kinetic energy.[24] It may be understood in a one-electron model as arising from the two-orbital four-(three-)electron destabilizing interactions between occupied orbitals on the two fragments.

In addition to the steric repulsion term ΔE^0, which is usually repulsive at the equilibrium distance since the repulsive component ΔE_{Pauli} dominates, attractive orbital interactions arise when the wavefunction ψ^0 is allowed to relax to the fully converged ground-state wavefunction of the total molecule, ψ^{AB}. The energy lowering due to mixing of virtual orbitals of the fragments into the occupied orbitals is called the electronic interaction energy $\Delta E_{\text{oi}}(=E^{AB} - E^0)$. This term, according to the decomposition scheme proposed by Ziegler and Rauk,[25] which is very useful for purposes of analysis, may be broken down into contributions from the orbital interactions within the various irreducible representations Γ of the overall symmetry group of the system, as in equation (6).

$$\Delta E = \Delta E^0 + \Delta E_{\text{oi}} = \Delta E^0 + \Sigma_\Gamma \Delta E(\Gamma) \quad (6)$$

In order to keep the calculations tractable, the tetraanionic unsubstituted porphyrinogen ligand L^{4-} was used and thf has been replaced by an appropriate OH_2 fragment. For $\eta^5,\sigma,\eta^5,\sigma$-[ZrL], bond distances and angles have been derived from X-ray structural data[8] and appropriately averaged to preserve a C_{2v} symmetry. The structure of σ,σ,σ,σ-[ZrL] was derived from that of $\eta^5,\sigma,\eta^5,\sigma$-[ZrL], by bending forward the η^5 pyrrolyls, keeping the four nitrogens in the same plane (*xy* plane in our coordinate system). The angle σ-pyrrolyl(centroid)–Zr–σ-pyrrolyl(centroid) was fixed at 164.5°, as in the case of $\eta^5,\sigma,\eta^5,\sigma$-co-ordination. The zirconium atom was again placed at $z = -0.57\ a_0$ and the C_{2v} symmetry was retained. The Zr–O distance in $\eta^5,\sigma,\eta^5,\sigma$-[ZrL]·$OH_2$ was derived from experiment while the Zr–H distance in $\eta^5,\sigma,\eta^5,\sigma$-[ZrL]·$H^-$ was optimized.

Table 1 Percentage contributions of individual atoms to relevant molecular orbitals (MOs) (based on Mulliken population analysis per MO). Only the most relevant contributing atomic orbitals (AOs) are indicated. For the atom labelling see Fig. 1 *

M		*E*/eV	N^1	N^2	C^{α}	C^{β}	$C^{\alpha'}$	$C^{\beta'}$	C^{b}	H
(*a*) $\eta^5,\sigma,\eta^5,\sigma$-L										
A_1	$14a_1$	−8.14	10.7 (p_z)	2.9	14.8 ($p_{y,z}$)	17.1 ($p_{y,z}$)	1.4	9.6 (p_y)	26.0	17.5
	$15a_1$	−6.36	55.4 (l.p.)	10.2 (p_y)	6.1 (p_x)	24.9 ($p_{x,z}$)	2.0	1.4	0.0	0.0
	$16a_1$	−6.00	14.8 (s, p_x)	26.7 (p_y)	1.0	2.2	5.5	47.8 (p_y)	0.0	2.0
	$17a_1$	−5.61	42.4 (l.p.)	4.9	2.2	45.8 (p_z)	0.0	4.7	0.0	0.0
	$18a_1$	−5.06	2.0	75.0 (l.p.)	0.0	0.0	7.8 (p_z)	6.9 (p_z)	4.4	3.9
A_2	$11a_2$	−5.62	0.0	0.0	24.3 ($p_{x,y}$)	7.9 (p_z)	49.8 (p_y)	16.8 (p_y)	0.0	1.2
	$12a_2$	−4.70	0.0	0.0	36.7 (p_z)	17.2 (p_z)	20.5 (p_y)	9.1 (p_y)	7.9	7.8
B_1	$13b_1$	−6.63	48.0 (l.p.)	0.0	5.4	22.5 (p_x)	11.4 (p_y)	5.5	5.3	1.8
	$14b_1$	−5.67	41.7 ($p_{x,z}$)	0.0	2.6	49.0 (p_z)	3.9	0.0	0.0	2.8
	$15b_1$	−4.87	22.6 (l.p.)	0.0	3.7	2.3	48.6 (p_y)	22.8 (p_y)	0.0	0.0
B_2	$13b_2$	−5.69	0.0	38.9 (p_y)	0.0	0.0	4.0	57.1 (p_y)	0.0	0.0
	$14b_2$	−5.38	0.0	43.7 (l.p.)	32.9 (p_z)	10.6 (p_z)	5.0	5.8	1.0	1.0
	$15b_2$	−4.70	1.0	34.1 (l.p.)	28.1 (p_z)	13.8 (p_z)	3.2	3.0	6.9	9.9
(*b*) $\sigma,\sigma,\sigma,\sigma$-L										
A_1	$14a_1$	−8.83	7.9 (p_z)	2.3	12.0 ($p_{x,z}$)	18.6 (p_z)	8.1 (p_z)	16.0 ($p_{y,z}$)	19.1	16.0
	$15a_1$	−5.91	16.9 (l.p.)	44.7 (l.p.)	2.2	9.0 (p_z)	24.0 (p_z)	0.0	0.0	0.0
	$16a_1$	−5.67	30.5 ($p_{x,z}$)	13.2 (p_z)	3.7	30.5 ($p_{x,z}$)	1.9	13.0	1.7	1.0
	$17a_1$	−5.61	15.7 (s, $p_{y,z}$)	43.0 ($p_{z,y}$)	2.6	13.8 ($p_{x,z}$)	4.9	20.0 ($p_{z,y}$)	0.0	0.0
	$18a_1$	−4.62	58.4 (l.p.)	21.5 (l.p.)	3.9	7.6	2.0	3.6	3.0	0.0
A_2	$11a_2$	−5.51	0.0	0.0	47.2 ($p_{z,y}$)	18.8 ($p_{x,z}$)	24.0 ($p_{z,x,y}$)	8.0 (p_y)	0.0	2.0
	$12a_2$	−5.28	0.0	0.0	18.0 (p_z)	7.5 (p_z)	39.0 ($p_{y,z}$)	18.4 ($p_{y,z}$)	2.8	6.2
B_1	$13b_1$	−5.66	39.4 ($p_{x,z}$)	0.0	5.4	53.5 ($p_{x,z}$)	0.0	0.0	0.0	1.7
	$14b_1$	−5.39	1.0	0.0	2.3	0.0	64.1 (p_z)	28.4 (p_z)	0.0	4.2
	$15b_1$	−4.87	80.2 (l.p.)	0.0	6.6 (p_x)	9.7	1.5	0.0	1.0	1.0
B_2	$13b_2$	−5.86	0.0	30.7 ($p_{y,z}$)	18.0	6.0	3.4	40.8 ($p_{y,z}$)	0.0	1.1
	$14b_2$	−5.41	0.0	78.4 (l.p.)	1.7	0.8	6.4	9.1 (p_y)	0.0	3.6
	$15b_2$	−5.29	0.0	13.1 (p_z)	43.1 (p_z)	19.5 ($p_{x,z}$)	2.3	11.5 (p_z)	2.7	7.8

* l.p. = lone pair.

Results and Discussion

Electronic Interactions in $\eta^5,\sigma,\eta^5,\sigma$- *and* $\sigma,\sigma,\sigma,\sigma$-[ZrL].—In this section we describe the electronic structure of $\eta^5,\sigma,\eta^5,\sigma$- and $\sigma,\sigma,\sigma,\sigma$-[ZrL] in terms of L^{4-} and Zr^{4+} fragments which are the most natural ones to build from these complexes. We will show later that this is a good assumption. For a proper understanding of the interaction it is important to look at the most relevant valence orbitals of the L ligand fragments in the $\eta^5,\sigma,\eta^5,\sigma$ and $\sigma,\sigma,\sigma,\sigma$ C_{2v} geometrical configurations they assume in the complexes. The atomic composition and the energy of these orbitals is given, separately for each symmetry, in Table 1 and refer to the ground state of the neutral ligand fragments. We will consider first the $\eta^5,\sigma,\eta^5,\sigma$-L fragment. As shown in Table 1, the orbitals of A_1 symmetry are well adapted for σ interactions with the metal, particularly the $15a_1$ and $17a_1$. These orbitals, being largely composed by σ-pyrrolyl nitrogen lone pairs with some contribution from η^5-pyrrolyl nitrogen p_y are suitable for interaction with a $d_{x^2-y^2}$ metal orbital. The N^1 p_x and N^2 p_y components of $16a_1$ make this orbital able to interact with the collar of the Zr d_{z^2}. On the other hand the A_2-type $11a_2$ and $12a_2$ MOs can provide only π interactions between the η^5 pyrrolyls and the d_{xy} metal orbital. Both in fact are mainly located on $C^{\alpha'}$ and $C^{\beta'}$ p_y AOs. The B_1 orbitals reported in the Table are σ like and except for the $15b_1$ which contains a large percentage of the $C^{\alpha'}$ and $C^{\beta'}$ p_y orbitals, are essentially located on σ pyrrolyls. Owing to their composition, the B_1 set of orbitals is well adapted for interaction with Zr d_{xz}. While the B_1-type valence orbitals interact with the metal only through the σ pyrrolyls, the η^5 pyrrolyls play the main role in the interactions that involve the B_2-type orbitals. The π-bonding ability of the η^5 pyrrolyls is mainly due to the π^* $13b_2$ and, to a lesser extent, the low-lying $11b_2$ π-pyrrolyl orbitals. Both these orbitals are properly directed to interact with Zr d_{xz}. The $15b_2$, largely a N^2 lone-pair orbital, is only able to combine in a σ fashion with the $5p_y$ orbital of the metal.

On going from $\eta^5,\sigma,\eta^5,\sigma$ to $\sigma,\sigma,\sigma,\sigma$ configuration, the electronic structure of the porphyrinogen ligand is modified to some extent, as inferred from the energy and the composition of the orbitals reported in Table 1, particularly the A_1-type orbitals. Due to the bending forwards of the η^5-pyrrolyl rings, N^1 and N^2 lone-pair combinations become mixed, as is found for $15a_1$ and $18a_1$ orbitals. The strong nitrogen lone-pair character makes these orbitals very suitable for σ interaction with Zr $d_{x^2-y^2}$, which is somewhat reminiscent of the σ interaction between metal and pyrrolyl nitrogens in porphyrin-like metallomacrocycles.[26] The remaining A_1-type orbitals do not substantially modify their nature, except for $17a_1$ which is no longer a N^1 lone-pair orbital. The composition of the $11a_2$ and $12a_2$ π-like MOs, which in $\eta^5,\sigma,\eta^5,\sigma$ configuration are directed towards the d_{xy} metal orbital, remain almost unchanged on going to $\sigma,\sigma,\sigma,\sigma$ configuration. However, owing to the configurational change of the η^5-pyrrolyls the overlap of these orbitals with Zr d_{xy} is no longer very effective.

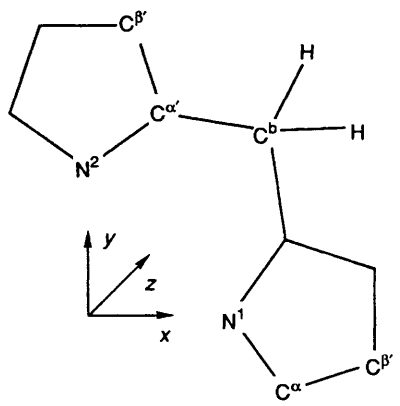

Fig. 1 Atom labelling scheme. In the case of $\eta^5,\sigma,\eta^5,\sigma$ co-ordination, N^1 and N^2 refer to the η^5 and σ pyrrolyls respectively. Zr is at x = 0.0, $y = 0.0$, $z = -0.57\ a_0$

Table 2 Percentage contribution of Zr^{4+} and L^{4-} fragment orbitals to MOs (based on Mulliken population analysis per MO) of $\eta^5,\sigma,\eta^5,\sigma$-[ZrL]. Only the most relevant ligand fragment orbitals are specified in parentheses

		Percentage Zr^{4+} atomic orbitals			Percentage L^{4-} fragment orbitals
	E/eV	s	p	d	
Unoccupied orbitals					
$22a_1$	−0.75	20.3	0.0	46.0 ($x^2 - y^2$,z^2)	33.7 [10.6 ($21a_1$), 6.5 ($20a_1$)]
$13a_2$	−1.84			57.2 (xy)	42.8 [9.2 ($11a_2$), 13.7 ($12a_2$), 14.5 ($15a_2$)]
$17b_2$	−2.52		0.0	72.6 (yz)	27.4 [14.4 ($13b_2$), 5.0 ($15b_2$), 5.5 ($17b_2$)]
$17b_1$	−2.86		0.0	63.0 (xz)	37.0 [7.8 ($14b_1$), 10.5 ($15b_1$), 8.9 ($16b_1$)]
$21a_1$	−3.24	34.0	1.6 (p_z)	43.2 (z^2)	21.2 [8.8 ($16a_1$), 5.0 ($21a_1$)]
Occupied orbitals					
$12a_2$	−4.36			2.8 (xy)	97.2 [29.9 ($11a_2$), 67.0 ($12a_2$)]
$16b_2$	−4.38		0.0	0.8 (yz)	99.2 [34.3 ($14b_2$), 62.6 ($15b_2$)]
$16b_1$	−5.64		0.0	0.0	100.0 [62.4 ($14b_1$), 32.2 ($15b_1$)]
$20a_1$	−5.72	0.0	0.0	0.0	100.0 [28.1 ($15a_1$), 65.5 ($17a_1$)]
$15b_1$	−6.27		0.0	15.0 (xz)	85.0 [8.9 ($11b_1$), 8.9 ($13b_1$), 14.8 ($14b_1$), 49.1 ($15b_1$)]
$19a_1$	−6.36	3.0	0.0	0.0	97.0 [89.6 ($18a_1$)]
$15b_2$	−6.40		2.0 (p_y)	0.9 (yz)	97.1 [61.0 ($14b_2$), 27.1 ($15b_2$)]
$11a_2$	−6.92			3.7 (xy)	96.3 [75.7 ($10a_2$), 12.9 ($11a_2$)]
$14b_1$	−7.10		0.0	0.0	100.0 [97.2 ($12b_1$)]
$10a_2$	−7.15			16.8 (xy)	83.1 [22.7($10a_2$), 43.0 ($11a_2$), 10.0 ($12a_2$)]
$13b_1$	−7.35		5.7 (p_x)	0.0	94.3 [72.4 ($13b_1$), 10.7 ($14b_1$)]
$14b_2$	−7.62		0.0	12.0 (yz)	88.0 [6.0 ($12b_2$), 74.0 ($13b_2$)]
$18a_1$	−7.85	0.0	0.0	6.0 (z^2)	94.0 [41.0 ($14a_1$), 42.0 ($16a_1$)]
$17a_1$	−8.13	0.0	1.0	8.0 (z^2)	91.0 [49.4 ($14a_1$), 36.9 ($16a_1$)]
$13b_2$	−8.55		0.0	2.2 (yz)	97.8 [82.4 ($12b_2$), 5.0 ($11b_2$)]
$12b_1$	−8.55		0.0	4.1 (xz)	95.9 [87.0 ($11b_1$), 4.4 ($13b_1$), 2.0 ($15b_1$)]
$16a_1$	−8.58	2.8	0.0	15.0 ($x^2 - y^2$)	67.2 [47.1 ($15a_1$), 16.8 ($17a_1$)]
$15a_1$	−8.89	2.8	0.0	1.0 ($x^2 - y^2$)	99.0 [84.1 ($13a_1$)]
$12b_2$	−8.94		0.0	3.2 (yz)	96.8 [14.8 ($9b_2$), 69.8 ($11b_2$)]
$9a_2$	−9.21			2.4 (xy)	97.6 [92.6 ($9a_2$)]
$9b_2$	−11.08		7.8 (p_y)	1.9 (yz)	90.3 [42.1 ($9b_2$), 31.5 ($10b_2$), 13.6 ($11b_2$)]
$12a_1$	−11.52	3.1	0.0	4.0 ($x^2 - y^2$)	92.9 [26.8 ($8a_1$), 28.3 ($10a_1$), 30.7 ($12a_1$)]

The B_1-type orbitals are still well adapted for σ bonding to the d_{xz} and p_x metal orbitals *via* N^1 lone pairs, the only significant effect of the change from $\eta^5,\sigma,\eta^5,\sigma$ to $\sigma,\sigma,\sigma,\sigma$ configuration being the inversion of $13b_1$ with $15b_1$. From Table 1 is is immediately apparent that, except for a greater localization on N^2, the B_2-type orbitals are not affected by the change in configuration. It should be noted however that they are no longer available for π bonding to the metal. The π* $13b_2$, which is suitable for interaction with the d_{yz} orbital in the $\eta^5,\sigma,\eta^5,\sigma$ co-ordination mode, is now unable to interact with the metal. On the other hand the $14b_2$ which is to a large extent a N^2 lone-pair orbital is now well suited for overlap with the d_{yz} orbital.

We now describe the electronic structure of the $\eta^5,\sigma,\eta^5,\sigma$-[ZrL] complex. The main metal–ligand interactions can be read from the Mulliken population analysis given in Table 2 in terms of Zr^{4+} and L^{4-} orbitals. We feel that the population of these fragment orbitals is more informative than the usual populations of primitive basis functions, particularly when one is interested in describing metal–ligand bonding.

The ground state of $\eta^5,\sigma,\eta^5,\sigma$-[ZrL] is unambiguously $^1A_2$. The energy gap between the highest occupied molecular orbital (HOMO) and lowest-unoccupied molecular orbital (LUMO) is however small (1.12 eV) and the LUMO, which is heavily metallic in nature, lies at quite low energy (−3.24 eV) making this molecule co-ordinatively unsaturated and highly reactive. Actually, it only exists when stabilized by interaction with a fifth ligand such as thf, H^-, or σ-alkyl fragments. The LUMO, being hybridized along the *z* axis away from the η^5 pyrrolyls, as it is clearly visible on the orbital plots of Fig. 2, will be the main contributor in the interaction with other σ-donor ligands or fragments. It is to be noted that this orbital is very similar in shape and composition to the well known $2a_1$ dsp hybrid reported by Hoffman and Lauher[27] for bent $M(C_5H_5)_2$ (M = Ti or Zr) fragments. As shown in Table 2, the $12a_2$ HOMO is, analogously to the highest occupied orbitals, mainly ligand-like, while the lowest orbitals of the virtual spectrum are strongly metallic in nature.

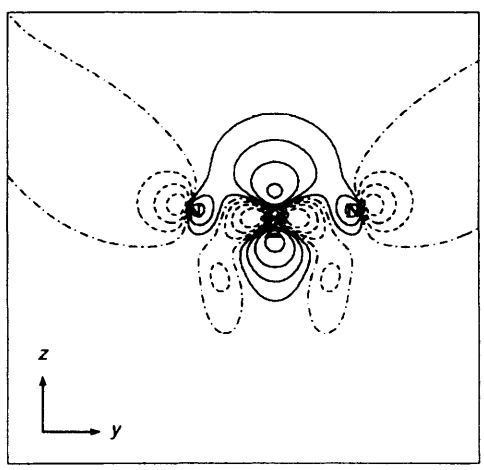

Fig. 2 Contour plot of the $\eta^5,\sigma,\eta^5,\sigma$-[ZrL] $21a_1$ LUMO orbital in the *yz* plane. Contour values are 0.0, ±0.02, ±0.05, ±0.1, ±0.2, ±0.5 $(e\ a_o^{-3})^{\frac{1}{2}}$

The metal orbitals of A_1 symmetry mix with several ligand MOs; however, the most significant mixing occurs in the low lying $16a_1$ MO where 18% of the metal orbitals (mainly $d_{x^2-y^2}$ with some 5s) interact, as expected, mostly with $15a_1$ and to a lesser extent with $17a_1$ ligand orbitals. As it is clearly depicted in Fig. 3(*a*), the $d_{x^2-y^2}$ metal orbital interacts in a σ fashion with the N^1 lone pair and with the N^2 p_y orbitals. The antibonding counterpart of $16a_1$ is the high lying $22a_1$ MO which has a large metal contribution (67%). There are other important interactions in this symmetry occurring in the $17a_1$ and $18a_1$ MOs.

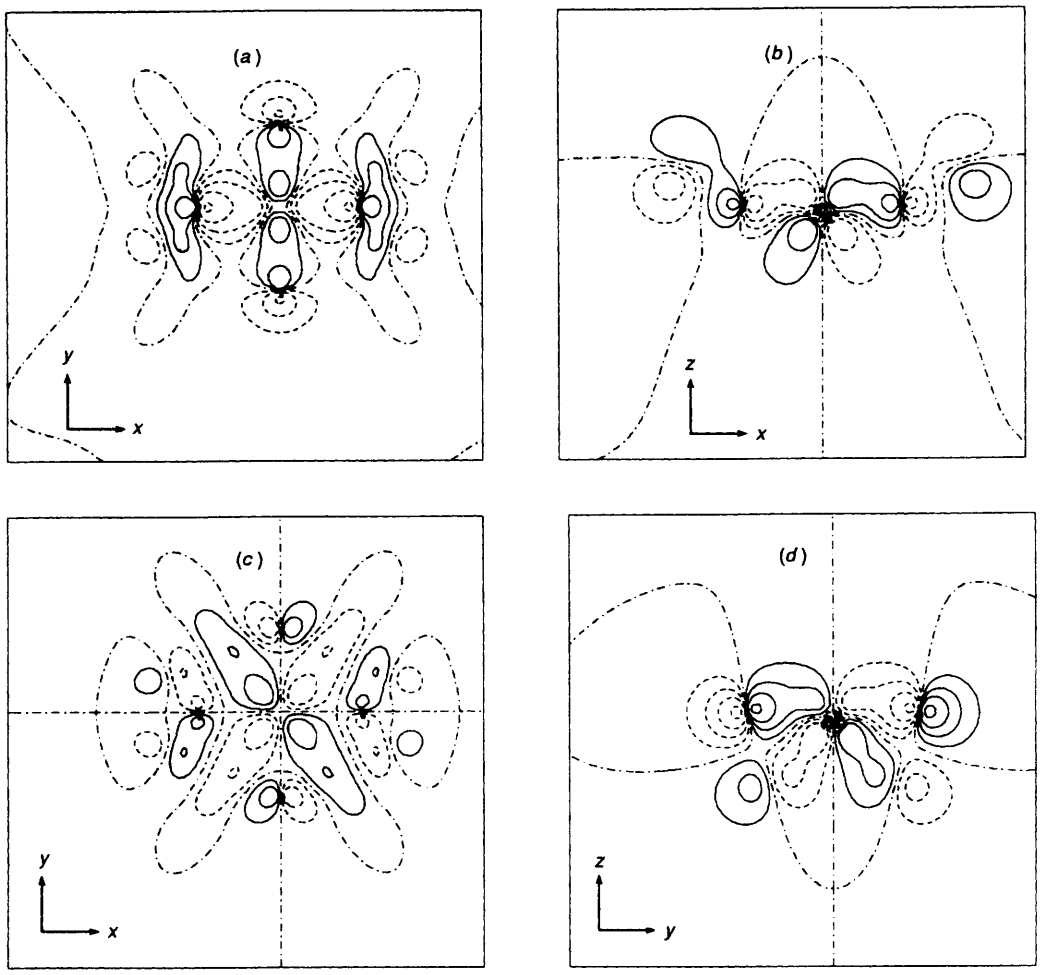

Fig. 3 Contour plot of relevant $\eta^5,\sigma,\eta^5,\sigma$-[ZrL] MOs: (*a*) $16a_1$, (*b*) $15b_1$, (*c*) $10a_2$, (*d*) $14b_2$. Contour values as for Fig. 2

These involve the d_{z^2} and the $16a_1$ ligand MO pointing towards the collar of this metal orbital. In the low lying $12a_1$ MO the $d_{x^2-y^2}$ and a small 5s component mix with the $12a_1$ fragment orbital which is primarily composed of p_y N^2 AOs.

In A_2 symmetry the main interaction occurs in the $10a_2$ MO where there is a π bond [see Fig. 3(*c*)] between Zr d_{xy} and $11a_2$, $12a_2$ π-ligand orbitals. The antibonding counterpart of $10a_2$ is $13a_2$ which is again metal centred (57.2%).

We have already stressed that in B_1 symmetry only the σ pyrrolyls would be involved in bonding with the metal. Actually, the largest metal–ligand mixing occurs in the $15b_1$ which is a mixture of the Zr d_{xz} orbital (15%) and $14b_1$, $15b_1$ ligand orbitals. The σ-bonding nature of this interaction is strikingly displayed in Fig. 3(*b*). The largely metallic $17b_1$ MO is the antibonding equivalent. As inferred from the populations reported in Table 2, there is some mixing of Zr $5p_x$ AO into L σ orbitals of B_1 symmetry.

As expected, the interactions occurring in B_2 symmetry only involve the η^5 pyrrolyls. The Zr d_{yz} mixes in $14b_2$ [see Fig. 3(*d*)] with a $\pi^*(13b_2)$-ligand orbital. In addition the Zr $5p_y$ AO is strongly stabilized by σ interaction with the N^2 p_y orbital.

On considering the electronic structure of $\sigma,\sigma,\sigma,\sigma$-[ZrL], from the energy and composition of the orbitals reported in Table 3, the small (only 0.22 eV) HOMO–LUMO gap is immediately apparent. Together with the lowering of energy of the LUMO this renders the complex highly reactive, much more so than $\eta^5,\sigma,\eta^5,\sigma$-[ZrL]. Again, the $21a_1$ LUMO orbital is well adapted for σ interaction with a fifth ligand. However, unlike the $\eta^5,\sigma,\eta^5,\sigma$ co-ordination mode, steric hindrance of N^2 lone pairs will no longer prevent the approach of a bulky ligand along the *z* axis. The overall orbital pattern of $\sigma,\sigma,\sigma,\sigma$-[ZrL] does not differ significantly from that found for $\eta^5,\sigma,\eta^5,\sigma$-[ZrL]; again, the highest occupied orbitals are mainly ligand centred, while the lowest virtual ones are largely metallic in nature.

The composition of the A_1 type orbitals indicates that the most significant mixing occurs in the $15a_1$ MO, where the Zr $d_{x^2-y^2}$ orbital interacts (13%) in a σ fashion with the N^1 and N^2 lone pairs, both available in this co-ordination mode. The remaining metal orbitals of A_1 symmetry, *i.e.* d_{z^2}, 5s and p_z, also mix with the ligand, particularly in the $16a_1$ and $19a_1$ MOs, but to a much lesser extent.

The interactions which occur in A_2 symmetry change significantly on going from $\eta^5,\sigma,\eta^5,\sigma$ to $\sigma,\sigma,\sigma,\sigma$ co-ordination. In fact only the $11a_2$ ligand orbital is still suitable for interaction with the d_{xy} orbital of the metal, allowing some mixing in the $11a_2$ MO. However the overlap is very weak (computed overlap integral 0.03), with the $11a_2$ fragment orbital located on the π-ring system of the η^5 pyrrolyls. Instead it is well suited for overlap with the d_{xy} orbital when the pyrrolyls are bent back, as in the case for the $\eta^5,\sigma,\eta^5,\sigma$ co-ordination. We can use the same argument to explain the behaviour of the $12a_2$ ligand orbital in this co-ordination. The consequence is a much lower d_{xy} population (0.5649 in $\eta^5,\sigma,\eta^5,\sigma$ *vs.* 0.2848 in $\sigma,\sigma,\sigma,\sigma$). Therefore, one would expect this interaction to be much stronger for $\eta^5,\sigma,\eta^5,\sigma$ co-ordination which is in fact the case as will be seen from the discussion of the energetic contribution of the A_2 interactions.

The change of co-ordination mode does not affect the nature of the B_1 type interactions. Again the Zr d_{xz} orbital mixes (17%) in a bonding fashion with N^1 p_x in the $15b_1$ MO, having the largely metallic $17b_1$ as its antibonding counterpart. Also the

Table 3 Percentage contribution of Zr^{4+} and L^{4-} fragment orbitals to MOs (based on Mulliken population analysis per MO) of σ,σ,σ,σ-[ZrL]. Only the most relevant ligand fragment orbitals are specified in parentheses

		Percentage Zr^{4+} atomic orbitals			Percentage L^{4-} fragment orbitals
	E/eV	s	p	d	
Unoccupied orbitals					
$18b_2$	−0.86		3.7 (p_y)	0.0	96.3 [88.7 ($16b_2$), 6.0 ($17b_2$)]
$22a_1$	−1.40	2.6	21.0 (p_z)	9.3 ($x^2 - y^2$)	67.0 [3.2 ($15a_1$), 3.0 ($16a_1$), 7.3 ($18a_1$), 49.8 ($19a_1$), 2.0 ($20a_1$)]
$17b_2$	−3.60		3.2 (p_y)	77.6 (yz)	19.2 [2.5 ($13b_2$), 7.5 ($14b_2$), 9.6 ($15b_2$)]
$17b_1$	−3.71		0.0	72.6 (xz)	27.4 [22.7 ($13b_1$), 1.5 ($14b_1$), 2.1 ($16b_1$)]
$13a_2$	−3.97			83.4 (xy)	16.6 [1.4 ($10a_2$), 7.9 ($11a_2$), 3.8 ($12a_2$)]
$21a_1$	−4.63	25.4	0.0	67.4 (z^2)	7.2 [1.5 ($15a_1$), 2.4 ($16a_1$), 1.8 ($19a_1$)]
Occupied orbitals					
$12a_2$	−4.85			0.0	100.0 [39.4 ($11a_2$), 60.5 ($12a_2$)]
$16b_2$	−4.88		0.0	2.1 (yz)	97.9 [17.2 ($13b_2$), 5.2 ($14b_2$), 75.1 ($15b_2$)]
$16b_1$	−5.33		0.0	0.0	100.0 [95.0 ($14b_1$), 1.8 ($15b_1$), 1.4 ($13b_1$)]
$11a_2$	−5.44			10.6 (xy)	89.4 [35.5 ($10a_2$), 52.5 ($11a_2$)]
$20a_1$	−6.13	0.0	0.0	0.0	100.0 [2.7 ($14a_1$), 13.8 ($15a_1$), 33.7 ($16a_1$), 43.0 ($17a_1$)]
$19a_1$	−6.52	0.0	1.6 (p_z)	3.6 (z^2)	94.8 [2.3 ($14a_1$), 5.0 ($15a_1$), 53.0 ($16a_1$), 30.0 ($17a_1$)]
$15b_2$	−6.52		0.6 (p_y)	5.6 (yz)	93.8 [1.6 ($11b_2$), 3.2 ($12b_2$), 73.7 ($13b_2$), 12.6 ($15b_2$)]
$15b_1$	−6.54		0.0	16.9 (xz)	83.1 [9.4 ($11b_1$), 68.1 ($13b_1$), 1.9 ($16b_1$)]
$14b_1$	−7.82		2.6 (p_x)	0.5 (xz)	97.0 [27.7 ($12b_1$), 61.5 ($15b_1$)]
$10a_2$	−8.02			1.3 (xy)	98.7 [97.2 ($10a_2$)]
$13b_1$	−8.30		2.0 (p_x)	0.0	98.0 [70.6 ($12b_1$), 23.3 ($15b_1$)]
$14b_2$	−8.36		2.6 (p_y)	11.6 (yz)	85.8 [2.6 ($6b_2$), 5.8 ($11b_2$), 71.3 ($14b_2$)]
$18a_1$	−8.50	0.0	0.0	4.0 ($x^2 - y^2$)	96.0 [36.5 ($13a_1$), 31.1 ($14a_1$), 6.7 ($15a_1$), 3.0 ($17a_1$), 14.0 ($18a_1$)]
$17a_1$	−8.82	0.0	0.0	0.0	100.0 [33.5 ($13a_1$), 56.6 ($14a_1$), 2.5 ($16a_1$), 3.0 ($17a_1$)]
$13b_2$	−8.83		0.0	0.0	100.0 [93.3 ($12b_2$), 1.7 ($13b_2$)]
$12b_1$	−8.97		0.0	2.0 (xz)	98.0 [3.6 ($10b_1$), 86.8 ($11b_1$), 4.7 ($13b_1$)]
$12b_2$	−9.14		0.0	0.0	100.0 [2.6 ($8b_2$), 5.3 ($9b_2$), 2.7 ($10b_2$), 83.2 ($11b_2$), 4.8 ($14b_2$)]
$16a_1$	−9.19	5.8	0.0	4.5 (z^2)	89.7 [5.0 ($7a_1$), 11.8 ($12a_1$), 4.9 ($13a_1$), 35.6 ($15a_1$), 14.7 ($17a_1$)]
$15a_1$	−9.58	0.0	0.0	12.6 ($x^2 - y^2$)	84.7 [9.3 ($8a_1$), 9.2 ($11a_1$), 18.1 ($12a_1$), 7.3 ($13a_1$), 34.9 ($18a_1$)]

involvement of Zr $5p_x$ is only minor, as inferred from the population of this orbital reported in Table 4.

Considering the mixing occurring in B_2 symmetry, we note that the $14b_2$ orbital has a sizable metal contribution (14%), indicating that σ,σ,σ,σ co-ordination does not prevent metal–ligand interaction, although it is of quite different nature. Owing to the change in configuration of the η^5 pyrrolyls, the π* ($13b_2$) ligand orbital which is the main contributor to the interaction with the metal in the η^5,σ,η^5,σ complex is now unable to overlap with the d_{yz} orbital. On the contrary, the new co-ordination mode brings the $14b_2$ N^2 lone-pair ligand orbital into play. For the same reason, the Zr $5p_y$ orbital is not suited for overlap with either the N^2 lone pair, or the N^2 p_y orbital, resulting in a dramatic decrease in the population of this orbital on going from η^5,σ,η^5,σ to σ,σ,σ,σ co-ordination.

The orbital interactions discussed above for the two co-ordination modes are reflected in the gross population data reported in Table 4. The largest charge transfer occurs in A_1 symmetry where 0.55 and 0.58 electrons respectively are donated to the $d_{x^2-y^2}$ orbital from ligand orbitals for η^5,σ,η^5,σ and σ,σ,σ,σ co-ordination respectively. The 5s population is mainly from L^{4-} orbitals, although a small amount is due to the mixing of 5s into d_{z^2} and $d_{x^2-y^2}$. The charge acquired by the d_{z^2} orbital comes essentially from the $16a_1$ fragment orbital which has the right symmetry to interact with the d_{z^2} collar. On going from η^5,σ,η^5,σ to σ,σ,σ,σ co-ordination we note a sizable lowering of the 5s and d_{z^2} populations. The contribution of $5p_z$ to the bond is almost negligible as inferred by its very small population.

In the η^5,σ,η^5,σ co-ordination mode there is a very large donation (0.56 electron) into the d_{xy} orbital from π-ligand orbitals ($11a_2$ and $12a_2$). As already stressed, for σ,σ,σ,σ co-ordination, the d_{xy} population is reduced by 50%. The σ interaction with N^1 lone pairs occurring in B_1 symmetry results in a donation into the d_{xz} orbital, which is quite large for both co-ordination modes.

Almost the same amount of charge is acquired by the d_{yz} orbital both in η^5,σ,η^5,σ and σ,σ,σ,σ co-ordination modes, although, as already discussed, this interaction is different in nature. Viewing η^5,σ,η^5,σ- and σ,σ,σ,σ-[ZrL] complexes as being composed from Z^{4+} and L^{4-} is justified by considering the final charge on the metal, 1.25 and 1.78 respectively. Charge has moved from the ligand to the metal which, as can be seen in the Mulliken analysis in Table 4, acquires 2.97 and 2.27 electrons in η^5,σ,η^5,σ- and σ,σ,σ,σ-[ZrL] complexes respectively. It is interesting that in the latter co-ordination mode the ligand-to-metal donation is somewhat smaller which enhances the σ-acceptor ability of the metal centre. The remaining charge rearrangements are due essentially to polarization.

Metal–Ligand Bond Strengths in η^5,σ,η^5,σ- *and* σ,σ,σ,σ-[ZrL] *Complexes.*—The charge rearrangements accompanying the bond formation are a qualitative indication of the relative strength of the metal–ligand interactions, but not a quantitative measure of their corresponding energies. These are explicitly calculated according to the energy decomposition scheme discussed before and displayed in Table 5 for both co-ordination modes. In order to have clear and meaningful energy contributions in the individual irreducible representations, we gave the fragments the ionic configurations L^{4-} (having the four extra electrons in A_2 and B_1 symmetry orbitals, *i.e.* $12a_2$ and $15b_1$) and $Zr^{4+}[(4d_{z^2})^0(4d_{x^2-y^2})^0(4d_{xy})^0(4d_{yz})^0(4d_{xz})^0(5s)^0]$. The Zr^{4+} and L^{4-} fragments for which the bonding energies are computed have been chosen to be in singlet states.

As shown in Table 5, the steric interaction energy ΔE^0 is strongly attractive in both complexes, due to the fact that the stabilizing contribution arising from the large attractive interaction between the charged fragments, ΔE_{elstat}, overcomes the positive (destabilizing) Pauli repulsion term, ΔE_{Pauli}.

As far as the orbital interaction energies are concerned, ΔE_{oi}, we would stress that as we are considering ionic interacting

Table 4 Mulliken gross population (electrons) of SCF orbitals of Zr^{4+} and L^{4-} fragments of $\eta^5,\sigma,\eta^5,\sigma$- and $\sigma,\sigma,\sigma,\sigma$-[ZrL]. All virtual orbitals of a given symmetry (other than the one given explicitly) are collectively denoted by a prefix *n*

	$\eta^5,\sigma,\eta^5,\sigma$-[ZrL]			$\sigma,\sigma,\sigma,\sigma$-[ZrL]		
A_1	Zr^{4+}	4s	2.0020	Zr^{4+}	4s	1.9975
		5s	0.3265		5s	0.1254
		$4p_z$	1.9985		$4p_z$	1.9995
		$5p_z$	0.0576		$5p_z$	0.0404
		$4d_{z^2}$	0.3546		$4d_{z^2}$	0.2356
		$4d_{x^2-y^2}$	0.5524		$4d_{x^2-y^2}$	0.5790
	L^{4-}	$11a_1$	1.9869	L^{4-}	$11a_1$	1.9899
		$12a_1$	1.8057		$12a_1$	1.9997
		$13a_1$	2.0000		$13a_1$	2.0000
		$14a_1$	1.9751		$14a_1$	1.9851
		$15a_1$	1.6661		$15a_1$	1.5992
		$16a_1$	1.6367		$16a_1$	1.8449
		$17a_1$	1.7592		$17a_1$	1.9143
		$18a_1$	1.8745		$18a_1$	1.4019
		n^*a_1	0.0190		n^*a_1	0.1550
A_2	Zr^{4+}	$4d_{xy}$	0.5649	Zr^{4+}	$4d_{xy}$	0.2848
	L^{4-}	$10a_2$	1.9946	L^{4-}	$10a_2$	1.9696
		$11a_2$	1.7692		$11a_2$	1.8403
		$12a_2$	1.6744		$12a_2$	1.9202
		n^*a_2	0.0063		n^*a_2	0.0761
B_1	Zr^{4+}	$4p_x$	1.9996	Zr^{4+}	$4p_x$	1.9989
		$5p_x$	0.0864		$5p_x$	0.0322
		$4d_{xz}$	0.4286		$4d_{xz}$	0.4791
	L^{4-}	$13b_1$	1.8389	L^{4-}	$13b_1$	1.5427
		$14b_1$	1.7983		$14b_1$	1.9638
		$15b_1$	1.7795		$15b_1$	1.8672
		n^*b_1	0.0438		n^*b_1	0.0913
B_2	Zr^{4+}	$4p_y$	2.0000	Zr^{4+}	$4p_y$	2.0000
		$5p_y$	0.1726		$5p_y$	0.075
		$4d_{yz}$	0.4302		$4d_{yz}$	0.4207
	L^{4-}	$9b_2$	1.9496	L^{4-}	$9b_2$	1.9996
		$10b_2$	1.9319		$10b_2$	1.9919
		$11b_2$	1.9000		$11b_2$	2.0000
		$12b_2$	1.9944		$12b_2$	1.9999
		$13b_2$	1.7308		$13b_2$	1.9211
		$14b_2$	1.9701		$14b_2$	1.7319
		$15b_2$	1.8539		$15b_2$	1.8064
		n^*b_2	0.0193		n^*b_2	0.0385

Table 5 Decomposition of the bonding energy (eV) of the complexes in terms of Zr^{4+} and L^{4-} ionic fragments

	$\eta^5,\sigma,\eta^5,\sigma$-[ZrL]	$\sigma,\sigma,\sigma,\sigma$-[ZrL]
ΔE_{elstat}	−74.89	−75.78
ΔE_{Pauli}	+12.58	+12.77
ΔE^0	−62.31	−63.01
ΔE_{A_1}	−14.19	−14.70
ΔE_{A_2}	−7.91	−4.90
ΔE_{B_1}	−8.37	−8.32
ΔE_{B_2}	−7.91	−7.65
ΔE_{oi}	−38.38	−35.57
$\Delta E^0 + \Delta E_{oi}$	−100.69	−98.58

fragments, polarization is expected to be important. Unfortunately this is not explicitly evaluable because the decomposition of energy contributions for different irreducible representations which we are using does not distinguish charge transfer and polarization. Looking at the different contributions to ΔE_{oi} it is immediately apparent that for both co-ordination modes the ΔE_{A_1} term is by far the strongest one, in line with the large donation occurring in this symmetry. We note that on going from $\eta^5,\sigma,\eta^5,\sigma$ to $\sigma,\sigma,\sigma,\sigma$ co-ordination this energy term increases slightly, in spite of the fact that σ donation into 5s and d_{z^2} drops by *ca.* 50%. This suggests that the metal–ligand σ interaction involving the $d_{x^2-y^2}$ orbital, whose population (see Table 4) is approximately the same in the two complexes, gives the major contribution to the ΔE_{A_1} term.

The contribution of the ΔE_{A_2} term is strikingly smaller in $\sigma,\sigma,\sigma,\sigma$- than in $\eta^5,\sigma,\eta^5,\sigma$-[ZrL], reflecting the population of Zr d_{xy} orbital for the two co-ordinations. The change in co-ordination has only a negligible effect on the ΔE_{B_1} and ΔE_{B_2} terms. For the former, this is not surprising as ΔE_{B_1} accounts for σ bonding from the metal to σ pyrrolyls (N^1 lone pairs). The constancy of ΔE_{B_2} term for both co-ordination modes indicates that changing the nature of the interactions does not change their strength. The total orbital-interaction contribution (the covalent component), ΔE_{oi} is strongly stabilizing in both co-ordination modes, although, because of the drop in the ΔE_{A_2} term, it is 2.8 eV smaller in $\sigma,\sigma,\sigma,\sigma$-[ZrL]. On comparing ΔE_{oi} and ΔE^0 terms, we note that the latter dominates. If we consider the steric term as a measure of the 'ionic' contribution to the bond, our results suggest that the formation of $\eta^5,\sigma,\eta^5,\sigma$- and $\sigma,\sigma,\sigma,\sigma$-[ZrL] complexes from Zr^{4+} and L^{4-} fragments is primarily an ionic process as approximately two thirds of the total bonding energy ($\Delta E_{oi} + \Delta E^0$) comes from the ionic term. The relative stability of $\eta^5,\sigma,\eta^5,\sigma$- and $\sigma,\sigma,\sigma,\sigma$-co-ordination modes is dominated by the ΔE_{A_2} term. In fact, the latter co-ordination is only 2.1 eV less stable, which is comparable with the lowering (2.8 eV) of ΔE_{A_2} term. On these grounds it is reasonable to predict the $\eta^5,\sigma,\sigma,\sigma$ and $\eta^3,\sigma,\eta^3,\sigma$ configurations to have intermediate stability. The small energy gap between the mixed $\eta^5,\sigma,\eta^5,\sigma$ co-ordination and the exclusively σ-co-ordination mode indicates that this change in configuration is a relatively easy process. The ^1H NMR spectrum [8] of $\eta^5,\sigma,\eta^5,\sigma$-[ZrL] indirectly supports the rather small energy barrier between the σ- and η^5-bonding mode of the pyrrolyl anions, as it shows that, while they are different at 293 K, they become equivalent at 313 K.

Concluding Remarks: σ and π Co-ordination Modes and Interaction with the Fifth Ligand in [ZrL] *Complexes.*—The theoretical analysis of the bonding modes of L^{4-} to a metal emphasises how to adapt either the number of electrons and/or the charge to the metal requirements, during a reaction pathway. The availability of a number of stable co-ordination modes is primarily due to the fact that the nitrogen lone pair and the π-ring system of the pyrrolyl act as both σ and π donors. In this respect the porphyrinogen ligand combines σ-donor abilities of porphyrins and π-donor abilities of cyclopentadienyls. The above bonding capabilities of pyrrolyl by itself would not provide, however, such a variety of co-ordination modes for L^{4-} ligands if they were not combined with the inherent flexibility of the porphyrinogen ring, which is determined by the breaking of delocalization at the bridge sites.

Whatever the co-ordination mode, the porphyrinogen ligand can stabilize high-valent unsaturated metal centres. Consequently $\eta^5,\sigma,\eta^5,\sigma$- and $\sigma,\sigma,\sigma,\sigma$-[ZrL] even more are suitable to interact with a fifth donor ligand approaching along the *z* axis. We have already recognized the $21a_1$ LUMO orbital of $\eta^5,\sigma,\eta^5,\sigma$-[ZrL] as the main contributor to these interactions. Experimentally it is well known that $\eta^5,\sigma,\eta^5,\sigma$-[ZrL] reacts [8a] with σ-donor ligands such as thf and H^- to yield $\eta^5,\sigma,\eta^5,\sigma$-[ZrL]·thf and $\eta^5,\sigma,\eta^5,\sigma$-[ZrL]·$H^-$. We shall analyse these interactions in detail.

As expected, the fully occupied H^- 1s orbital, $1a_1$ in C_{2v} symmetry, mixes strongly with the $21a_1$ LUMO orbital of $\eta^5,\sigma,\eta^5,\sigma$-[ZrL]. Due to a very efficient overlap (0.4826) of these orbitals, this interaction results in considerable σ donation (0.91 e) from $1a_1$ of the H^- fragment into the $21a_1$. Accordingly, as inferred from the energy data reported in Table 6, the ΔE_{A_1} term is large (−3.61 eV) and represents the most important contribution to the total bond energy (−3.94 eV). In fact, steric repulsion is low and the contributions of ΔE_{A_2}, ΔE_{B_1} and ΔE_{B_2} which account for polarization are very small.

The interaction with OH_2 fragment is much weaker than that with H^-. The total bonding energy ($\Delta E_{oc} + \Delta E^0$) is only −0.76 eV and reflects the lower value of the ΔE_{A_1} term. This is a consequence of the lower σ-donor ability of the ligand. Energy

Table 6 Decomposition of the bonding energy (eV) for the interaction of $\eta^5,\sigma,\eta^5,\sigma$-[ZrL] with OH_2 (at the experimental Zr–O distance 4.224 a_o) and H^- (at the optimized Zr–H distance 3.629 a_o)

	OH_2	H^-
ΔE_{elstat}	−2.78	−6.17
ΔE_{Pauli}	+2.94	+6.53
ΔE^0	+0.16	+0.36
ΔE_{A_1}	−0.70	−3.61
ΔE_{A_2}	−0.01	−0.19
ΔE_{B_1}	−0.11	−0.26
ΔE_{B_2}	−0.10	−0.24
ΔE_{oi}	−0.92	−4.30
$\Delta E^0 + \Delta E_{oi}$	−0.76	−3.94

mismatch prevents the OH_2 $2a_1$ donor orbital to mix with the $21a_1$ acceptor orbital of the complex, although their overlap is not negligible (0.2628). The low contribution of ΔE_{B_1} and ΔE_{B_2} terms indicates a negligible π interaction between the OH_2 fragment and the metal centre.

The above energy analysis indicates that (*i*) the interaction of $\eta^5,\sigma,\eta^5,\sigma$-[ZrL] with Lewis bases of quite different donor ability, *i.e.* OH_2 (thf) or H^- is a favoured process and (*ii*) the most stable co-ordination ($\eta^5,\sigma,\eta^5,\sigma$) of the complex is preserved, which is in reasonable agreement with the experimental findings.[8]

On theoretical grounds, one may predict that a change in co-ordination in the substrate would only occur in presence of a bulky fifth ligand, in order to relieve steric hindrance of the η^5-pyrrolyl nitrogen lone pairs. This suggestion finds some support in experimental evidence, as the reaction of $\eta^5,\sigma,\eta^5,\sigma$-[ZrL] with an alkyl ligand such as butyl yields $\eta^5,\sigma,\sigma,\sigma$-[ZrL]·$C_4H_9^-$.[8c]

Acknowledgements

We thank Professor E. J. Baerends for a copy of the newest version of the ADF program system. A. R. and G. R. thank the Centro Interfacotta Seruizi Informatica e Telematici of Universitá della Basilicata for access to their computing facilities.

References

1 *The Porphyrins*, ed. D. Dolphin, Academic Press, New York, 1978–79, vols. 1–7; K. M. Smith, *Porphyrins and Metalloporphyrins*, Elsevier, Amsterdam, 1975.

2 T. Mashiko and D. Dolphin, in *Comprehensive Coordination Chemistry*, eds. G. Wilkinson, R. Gillard and J. A. McCleverty, Pergamon, Oxford, 1987, vol. 2, ch. 21.1, p. 855; J. B. Kim, A. D. Adler and R. F. Longo, in *The Porphyrins*, ed. D. Dolphin, Academic Press, New York, 1978, vol. 1, part A, p. 85; D. Mauzerall, in *The Porphyrins*, ed. D. Dolphin, Academic Press, New York, 1978, vol 2, p. 91; B. von Maltzan, *Angew. Chem., Int. Ed. Engl.*, 1982, **21**, 785; J. S. Lindsey, I. C. Schreiman, H. C. Hsu, P. C. Kearney, and A. M. Marguerettaz, *J. Org. Chem.*, 1987, **52**, 827; J. S. Lindsey and R. W. Wagner, *J. Org. Chem.*, 1989, **54**, 828.

3 B. Franck, *Angew. Chem., Int. Ed. Engl.*, 1982, **21**, 343; J. E. Johansen, V. Piermattie, C. Angst, E. Diener, C. Kratky and A. Eschenmoser, *Angew. Chem., Int. Ed. Engl.*, 1981, **20**, 261; C. Kratky, R. Waditschatka, C. Angst, J. E. Johansen, J. C. Plaquevent, J. Schreiber and A. Eschenmoser, *Helv. Chim. Acta*, 1985, **68**, 1312; R. Waditschatka, E. Diener and A. Eschenmoser, *Angew. Chem., Int. Ed. Engl.*, 1983, **22**, 631; C. Angst, M. Jakiwara, E. Zass and A. Eschenmoser, *Angew. Chem., Int. Ed. Engl.*, 1980, **19**, 140; R. Waditschatka, C. Kratky, B. Jaun, J. Heinzer and A. Eschenmoser, *J. Chem. Soc., Chem. Commun.*, 1985, 1604; R. Waditschatka and A. Eschenmoser, *Angew. Chem., Int. Ed. Engl.*, 1983, **22**, 630; J. E. Johansen, C. Angst, C. Kratky and A. Eschenmoser, *Angew. Chem., Int. Ed. Engl.*, 1980, **19**, 141, 263.

4 H. Fischer and H. Orth, *Die Chemie des Pyrrols*, Akademische Verlagsgesellschaft m.b.H, Leipzig, 1934, p. 20; A. Baeyer, *Ber.*, 1886, **19**, 2184; M. Dennstedt and J. Zimmermann, *Ber.*, 1887, **20**, 850, 2449; 1888, **21**, 1478; M. Denstedt, *Ber.*, 1890, **23**, 1370; V. V. Chelintzev, and B. V. Tronov, *J. Russ. Phys. Chem. Soc.*, 1916, **48**, 105, 127; Th. Sabalitschka and H. Haase, *Arch. Pharm.*, 1928, **226**, 484; P. Rothemund, and C. L. Gage, *J. Am. Chem. Soc.*, 1955, **77**, 3340.

5 D. Jacoby, C. Floriani, A. Chiesi-Villa and C. Rizzoli, *J. Chem. Soc., Chem. Commun.*, 1991, 220.

6 J. Jubb, D. Jacoby, C. Floriani, A. Chiesi-Villa and C. Rizzoli, *Inorg. Chem.*, 1992, **31**, 1306.

7 J. Jubb, D. Jacoby, C. Floriani, A. Chiesi-Villa and C. Rizzoli, *J. Am. Chem. Soc.*, 1991, **114**, 6571.

8 (*a*) D. Jacoby, C. Floriani, A. Chiesi-Villa and C. Rizzoli, *J. Chem. Soc., Chem. Commun.*, 1991, 790; (*b*) *J. Am. Chem. Soc.*, 1993, **115**, 3995; (*c*) unpublished work.

9 A. Rosa and E. J. Baerends, *New J. Chem.*, 1991, **15**, 815 and refs. therein.

10 E. J. Baerends, D. E. Ellis and P. Ros, *Chem. Phys.*, 1973, **2**, 42; E. J. Baerends and P. Ros, *Chem. Phys.*, 1973, **2**, 51; E. J. Baerends and P. Ros, *Int. J. Quantum Chem.*, 1978, **S12**, 169.

11 P. M. Boerrigter, G. te Velde and E. J. Baerends, *Int. J. Quantum Chem.*, 1988, **33**, 87; G. Te Velde and E. J. Baerends, *J. Comput. Phys.*, 1992, **99**, 84.

12 R. G. Parr and W. Yang, *Density-Functional Theory of Atoms and Molecules*, Oxford University Press, New York, 1989.

13 S. H. Vosko, L. Wilk and M. Nusair, *Can. J. Phys.*, 1980, **58**, 1200.

14 H. Stoll, E. Golka and E. Preuss, *Theor. Chim. Acta*, 1980, **29**, 55.

15 A. D. Becke, *J. Chem. Phys.*, 1986, **84**, 4524.

16 T. Ziegler, V. Tschinke and C. Ursenbach, *J. Am. Chem. Soc.*, 1987, **109**, 4825.

17 T. Ziegler, V. Tschinke and A. Becke, *Polyhedron*, 1987, **6**, 685.

18 T. Ziegler, V. Tschinke and A. Becke, *J. Am. Chem. Soc.*, 1987, **109**, 1351; T. Ziegler, W. Cheng, E. J. Baerends and W. Ravenek, *Inorg. Chem.*, 1988, **27**, 3458; T. Ziegler, V. Tschinke, E. J. Baerends, J. G. Snijders and W. Ravenek, *J. Phys. Chem.*, 1989, **93**, 3050; T. Ziegler, E. J. Baerends and J. G. Snijders, *J. Chem. Phys.*, 1981, **74**, 5737.

19 T. Ziegler, V. Tschinke, L. Versluis, E. J. Baerends and W. Ravenek, *Polyhedron*, 1988, **7**, 1625.

20 K. Morokuma, *J. Chem. Phys.*, 1971, **55**, 1236.

21 T. Ziegler and A. Rauk, *Inorg. Chem.*, 1979, **18**, 1558, 1755.

22 H. Fujimoto, J. Osamura and T. Minato, *J. Am. Chem. Soc.*, 1978, **100**, 2954.

23 K. Kitaura and K. Morokuma, *Int. J. Quantum Chem.*, 1976, **10**, 325.

24 P. J. Van de Hoek, A. W. Kleyn and E. J. Baerends, *Comments At. Mol. Phys.*, 1989, **23**, 93.

25 T. Ziegler and A. Rauk, *Theor. Chim. Acta*, 1977, **46**, 1.

26 A. Rosa, G. Ricciardi, F. Lelj and Y. Chizhov, *Chem. Phys.*, 1992, **161**, 140; A. Rosa and E. J. Baerends, *Inorg. Chem.*, 1992, **31**, 4717; M. Zerner and M. Gouterman, *Theor Chim. Acta*, 1967, **8**, 26; P. A. Reynolds and B. N. Figgis, *Inorg. Chem.*, 1991, **30**, 2294.

27 J. W. Lauher and R. Hoffmann, *J. Am. Chem. Soc.*, 1975, **98**, 1729.

Received 28*th May* 1993; *Paper* 3/03065B